On the formation of antiphase boundaries in Fe_4Al_{13} intermetallics during a high temperature treatment

On the formation of antiphase boundaries in Fe_4Al_{13} intermetallics during a high temperature treatment

Lipeng Ding[a,b,c,*], Thaneshan Sapanathan[b,d], Dominique Schryvers[c], Aude Simar[b], Hosni Idrissi[b,c]

[a] Key laboratory for Light-weight Materials, Nanjing Tech University, Nanjing 211816, PR China

[b] UCLouvain, Institute of Mechanics Materials and Civil Engineering, IMAP, 1348 Louvain-la-Neuve, Belgium

[c] Electron Microscopy for Materials Science (EMAT), Department of Physics, University of Antwerp, 2020 Antwerp, Belgium

[d] Curtin Corrosion Centre, Faculty of Science and Engineering, Curtin University, Perth, WA 6102, Australia

Corresponding author: lipeng.ding@njtech.edu.cn

Abstract

In this paper, we report atomic scale observations and formation mechanisms of a high-density of antiphase boundaries (APBs) within an ultra-fine-grained Fe_4Al_{13} intermetallic layer at an Al/steel interface after a heat treatment at 596 °C. The results reveal that the APBs are formed by nucleation and the glide of partial dislocations with Burgers vector of b/3[010] (b=12.47 Å). The intensive activation of APBs locally transforms the Fe_4Al_{13} structure from the quasicrystal approximant structure to a quasicrystal. Very few stacking faults and nanotwins are observed indicating that the formation of planar defects is mainly driven by this transformation. This new insight on the formation of high density of APBs could possibly lead to an improvement in toughness by increasing the strength/ductility balance of this intermetallic.

Keywords: Al/steel interface; intermetallics; antiphase boundary; transmission electron microscopy

Iron aluminides are largely investigated systems as they spontaneously form during many modern engineering applications such as dissimilar welding, coating, hot dip aluminizing and fabrication of in situ composites [1]. Stable iron aluminide intermetallics with more than 50 at.% of aluminum ($FeAl_2$ – ζ, Fe_2Al_5 – η and Fe_4Al_{13} – θ also referred to as $FeAl_3$ in some early literature) exhibit very low toughness. $FeAl_2$ – ζ, Fe_2Al_5 – η and Fe_4Al_{13} – θ phases have a room temperature toughness of 0.59 MPa·$m^{1/2}$, 0.82 MPa·$m^{1/2}$ and 0.97 MPa·$m^{1/2}$, respectively [2]. This is attributed to the presence of strong covalent bonding, which makes dislocation motion difficult. To improve the ductility of the IMs, several strategies have been applied such as severe plastic deformation, introduction of nanotwins or bimodal microstructure [3]. However, most of these methods are a trade-off between strength and plasticity. It has also been demonstrated that planar defects generated during processing could play an important role to improve ductility by acting as sources for dislocations [4-6]. Therefore, understanding the elementary defect mechanisms is important to improve the strength-ductility balance in this class of materials.

Chen et al. [7] reported the formation of high-density of nanoscale planar defects including stacking faults and twins within the Fe_4Al_{13} phase in the molten aluminum/solid steel IM layer. Fung et al. [8] observed the presence of Fe_4Al_{13} tenfold twins and Al-Fe decagonal quasicrystal in a rapidly solidified Al-Fe alloy while Saito et al. [9] reported the existence of three kinds of twins, i.e. (001), (100) and (20-1) twin in the Fe_4Al_{13} phase. In Co_4Al_{13} phase, which is homeotypic with Fe_4Al_{13}, the formation of a high density of dislocations with [010] Burgers vector terminating (001) planar defects was observed during deformation [10]. Korte-Kerzel et al. [3] demonstrated that the plasticity at room temperature in the Co_4Al_{13} phase is controlled by the motion of metadislocations, which are highly complex partial dislocations mediating plasticity in various IMs. Anti-phase boundaries (APBs) are frequently observed in IMs with superlattice, such as Ni (Co)-based single crystal super alloy [11, 12]. However, to the best of the author's knowledge, such defects have rarely been directly observed for the Fe_4Al_{13} phase. In the present work, a high density of APBs formed within the Fe_4Al_{13} intermetallic is reported. Aberration corrected high resolution scanning

transmission electron microscopy (HRSTEM) is used to investigate the atomic scale characteristics of these defects as well as their formation mechanisms.

Friction Melt Bonding (FMB) process is used to obtain an Al/Fe interface with two intermetallics (Fe_2Al_5 and Fe_4Al_{13}). FMB is a recently developed process to weld dissimilar materials. More information on the FMB process can be found elsewhere [13, 14]. First, a dual phase (DP600) steel plate is placed on top of the aluminum. During FMB, the heat generated by the friction between the tool and the steel plate is sufficient to melt the aluminum. This facilitates reaction and diffusion between the liquid aluminum and solid steel leading to the formation of Fe_2Al_5 and Fe_4Al_{13} intermetallics at the interface [13, 15]. Scanning electron microscopy (SEM) observations were made on the transverse section of the FMB welded interface with secondary electrons using a ZEISS FEGSEM (Field emission gun scanning electron microscopy) Ultra 55 instrument. 300 µm thick specimens extracted from the interface zone containing both Fe_2Al_5 and Fe_4Al_{13} IMs, aluminum and steel, have been heat treated at 596 °C for 6 minutes. The temperature-time plot used during the heat treatment is given in Supplementary Fig. S1. This enabled the growth of the IMs. Cross-sectional TEM thin foils were also prepared using a dual-beam Scanning Electron Microscope/Focused Ion Beam (SEM/FIB) instrument (FEI Helios Nanolab 650) with the “lift-out” procedure. Bright-field TEM (BF-TEM) images and selected area electron diffraction (SAED) were acquired in a FEI Tecnai G2 F20 TEM operated at 200kV. A FEI Titan 80-300 “Cube” microscope with double aberration correctors (image and probe correction) was used to investigate the local atomic structure of the IM.

The SEM observation in Fig 1a shows that the IM layer formed after FMB at the Al/Steel interface exhibits an average thickness of 7.1 ± 1.5 µm. It can also be seen that this layer involves two different iron aluminides as separated by a white dotted line (Fig. 1a). Earlier investigations confirmed that Fe_2Al_5 is formed on the steel side while Fe_4Al_{13} is formed on the aluminum side [16]. Cross-sectional FIB lamellae are thus lifted out from the steel and aluminum side IM to investigate the Fe_2Al_5 and Fe_4Al_{13} phases

respectively. Significant microstructural changes were not detected in the existing Fe_2Al_5 phase after 596 °C heat treatment while the Fe_4Al_{13} phase yields some interesting microstructural changes as will be detailed later. TEM-BF images of the IMs before and after the heat treatment are presented in Figs. 1b and c, respectively. In Fig. 1b, the Fe_4Al_{13} IM exhibits grain sizes ranging from 1 to 2 µm with only few dislocations within the grains. After the 596°C heat treatment, the grains became more equiaxed with grain size between 100 nm and 500 nm (Fig. 1c). The SAED patterns obtained in the regions marked by white circles in Figs. 1b and c and shown in Figs. 1d and e, respectively, confirm the presence of the m-Fe_4Al_{13} phase with a monoclinic structure before and after the 596°C heat treatment. This was consolidated using SAED patterns acquired along other zone axes (see supplementary Fig. S2). TEM-EDX (Energy dispersive X-ray spectroscopy) measurements performed in the same regions support the identification of the Fe_4Al_{13} phase (Fig. 1f).

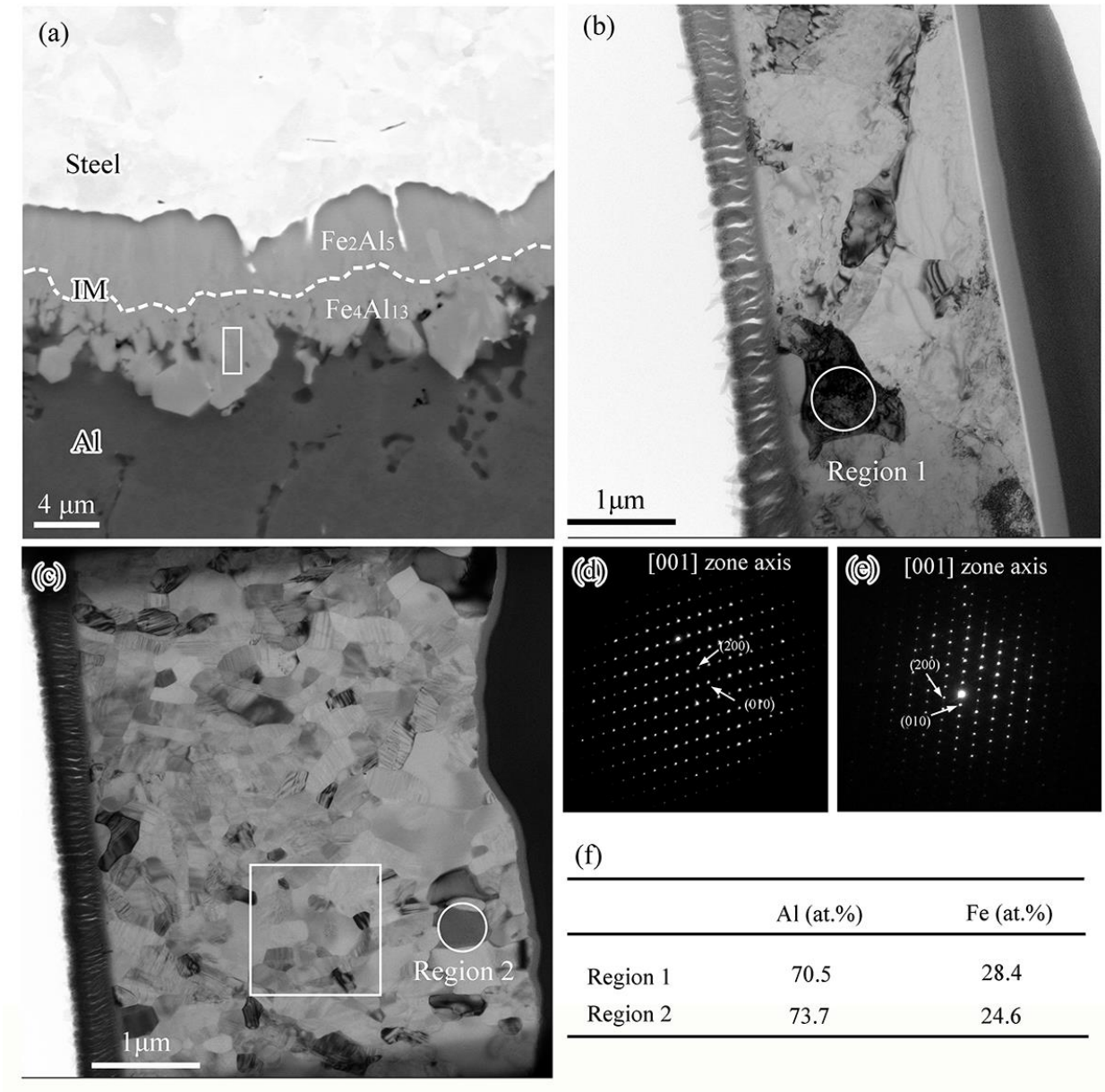

(f)

	Al (at.%)	Fe (at.%)
Region 1	70.5	28.4
Region 2	73.7	24.6

Fig. 1. (a) Backscattered SEM micrograph of the IMs formed at the Al/Steel interface after FMB. (b, c) TEM bright-field micrographs of the Fe_4Al_{13} phase formed at the interface before and after the 596°C heat treatment, respectively. The SAED patterns in (d) and (e) are obtained in the regions marked by the white circles in (b) and (c), respectively. (f) EDX results corresponding to the regions marked by white circles in (b) and (c). The white rectangle corresponds to the zone selected for detailed analysis in Figure 2.

Fig. 2a shows a magnified TEM-BF image in the area marked by the white rectangle in Fig. 1c. In this figure, most of the grains contain nanoscale parallel planar defects (see black arrows in Fig. 2a). The TEM-BF image of Fig. 2b shows that some planar defects are rather straight (red arrow) while others exhibit a more curved aspect (blue arrow). In the SAED pattern shown in the inset of Fig. 2b, diffraction spots with strong streaks are observed along the (010) plane, indicating the presence of edge-on planar defects parallel to this plane. Fig. 2c exhibits an HAADF-STEM image of the m-Fe_4Al_{13} phase without planar defects viewed along [001] zone axis. The monoclinic unit cell is marked by red lines in this figure. The m-Fe_4Al_{13} structure can be described by the tiling of two rhombs and a pentagon connected with a second pentagon rotated by 180°. This arrangement leads to a flat octagon-type substructure. Therefore, the Fe_4Al_{13} phase is considered as a decagonal quasicrystal approximant. The periodic arrangement of the octagon-type substructure can be schematized in Fig. 2d.

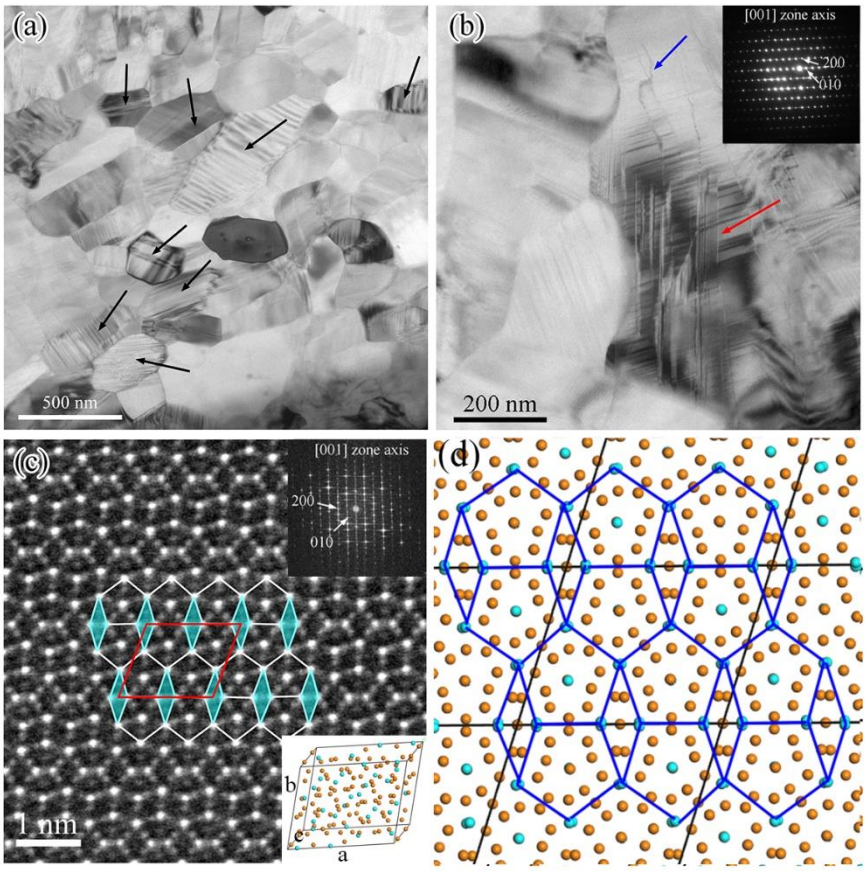

Fig. 2. (a and b) TEM bright-field images showing planar defects (black arrows in (a)) formed in the Fe_4Al_{13} intermetallic phase after the 596°C heat treatment. Straight and curved planar defects are marked by red and blue arrows, respectively. (c) HAADF-STEM image of the m-Fe_4Al_{13} phase without planar defects observed along [001] zone axis. The rhombs are light blue filled and the unit cell is marked by red lines. (d) Schematic illustration of the substructure of the Fe_4Al_{13} phase. The unit cell of Fe_4Al_{13} is marked by black lines while tiling octagons are highlighted by blue lines. The Fe and Al atoms are marked by blue and orange spheres, respectively.

Figs. 3a and 3d exhibit high resolution high angle annular dark-field scanning transmission electron microscopy (HAADF-STEM) images of the straight and curved planar defects shown in Fig. 2b, respectively. In these figures, the planar defects are marked by yellow lines while the unit cell of the m-Fe_4Al_{13} is indicated by red lines. Fig. 3b shows a magnified HAADF-STEM image of the region indicated by the blue square in Fig. 3a. The rhombs at the planar defect (orange filled zones) are rotated by ~45^o with respect to the rhombs in the matrix (blue filled zones). Detailed analysis of the arrangement of these rhombs confirms the presence of the o-Fe_4Al_{13} with orthorhombic structure at the planar defect. Therefore, the m-Fe_4Al_{13} can transform to o-Fe_4Al_{13} and then transform back to m-Fe_4Al_{13} in this defect. In the schematic illustration of Fig.3c, it can be seen that the planer defect is an anti-phase boundary (APB) formed by the translation of the m-Fe_4Al_{13} unit cell by b/3 [010] in the (100) plane leading to local transformation from m-Fe_4Al_{13} to o-Fe_4Al_{13} as reported in [9]. Besides, the formation of these APBs leads to the loss of the periodic arrangement of the m-Fe_4Al_{13} crystal leading to local transformation of the quasicrystal approximant into a quasicrystal. This is evidenced by the formation of a 5-fold symmetry pattern marked by the red circles in the FFT pattern inserted in the right corner of Fig. 3a [17], see also Fig. S3 in supplementary materials. In Fig.3d, the APB exhibits a 'zig-zag' morphology with planes switching from (100) and $(1\bar{1}0)$. Fig. 3e exhibits a magnified HAADF-STEM image of the APB segment indicated by the green square in Fig. 3d. In Fig.3e, a flat hexagon (light green filled zones) is formed when the APB switches from the (100) plane to the $(1\bar{1}0)$ plane. The schematic illustration of Fig. 3f shows the occurrence in this site of a translation of the m-Fe_4Al_{13} crystal by a/2 [100] in the (010) plane and b/3 [010] in the (100) plane. Furthermore, no dislocation is detected at the same site (see Supplementary Fig. S4).

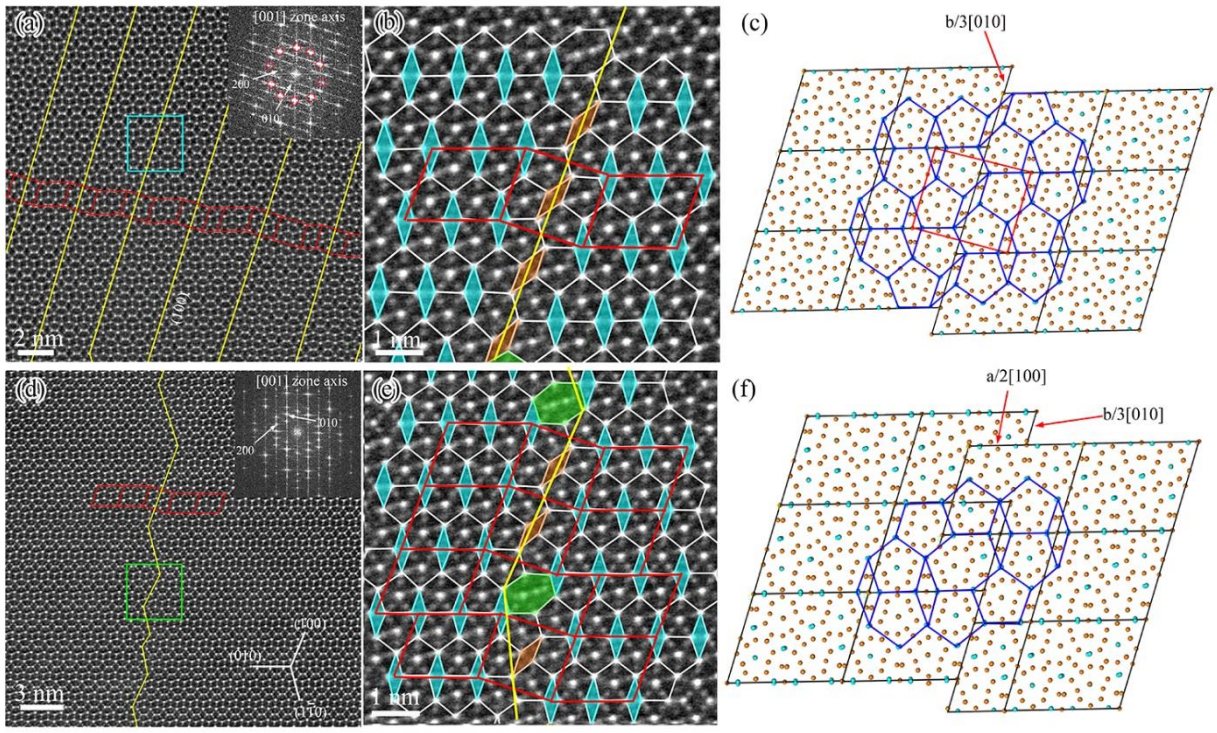

Fig. 3. (a and d) High resolution HAADF-STEM images of APBs in the m-Fe_4Al_{13} phase. The unit cells of the m-Fe_4Al_{13} are marked by red lines while the APBs are indicated by yellow lines. (b and e) Magnified HAADF-STEM images from the blue and green squares in (a and d), respectively. Tiling octagons are marked by white lines. The rhombs are filled by light blue and orange depending on their orientations. The 5-fold symmetry patterns are marked by the red circles in the FFT pattern. The flat hexagons in (e) are filled by light green. (c and f) Schematics illustrating explaining the formation of the APB within the m-Fe_4Al_{13} phase shown in (b) and (e).

The HAADF-STEM images of Fig. 4 show planar defects with larger thickness (green lines). Some APBs can also be observed in these images (yellow lines). In Fig. 4a, the planar defect indicated by green lines has a thickness of 7.5 nm, which is half the unit cell size of m-Fe_4Al_{13}. Fig. 4b shows an enlarged HAADF-STEM image from the blue square in Fig. 4a. It clearly shows that a row pentagon/rhomb tile (the rhombs are light yellow filled) are rotated by 107° with respect to the matrix. Therefore, this planar defect can be considered as a stacking fault (SF) [3]. Note here the difference between SF and APB. Indeed, the formation of a SF is associated with a row pentagon/rhomb tile (half unit cell of the m-Fe_4Al_{13}) twinned

with respect to the matrix [3], while APB causes local shift of the m-Fe_4Al_{13} unit cell by b/3 [010] in the (100) plane [8]. The nanoscale lamella delimited by the green lines in Fig. 4c is clearly identified as (100) twin stopping inside the grain [9]. The presence of streaking in the FFTs agrees with the observation of stacking faults and nanosized twins. In Fig. 4d, the magnified HAADF-STEM image from the blue square in Fig. 4c confirms that the formation of the (100) twin involves the formation four twin-like rows of pentagon/rhomb tiles (the rhombs are orange filled) rotated by 107°. A series of irregular polygons (marked by white lines) is formed at the tip of the twin (Fig. 4d). The local g-map inset in Fig. 4c was obtained using Geometric Phase Analysis (GPA) which is an image processing method sensitive to small displacements of the lattice fringes in high resolution TEM images. It reveals the presence of a dislocation at the tip of the twin, indicating the incoherent character of the twin front. The core of this dislocation is identified by a Burgers circuit using unstrained tiles (Fig. 4e). The Burgers vector is identified as $\mathbf{b} = b/\tau^5(010)$, with $|\mathbf{b}| = 0.113\text{nm}$, where $\tau = 1/2(\sqrt{5}+1)$. These observations show that different types of extended defects including APBs, stacking faults and twins have been formed in the Fe_4Al_{13} intermetallic after the 596°C heat treatment. It is worth noting that APBs dominate the microstructure, while stacking faults and twins only account for 1% of all the observed defects. This indicates that the APBs would play an important role in dictating the mechanical properties of the Fe_4Al_{13} intermetallic.

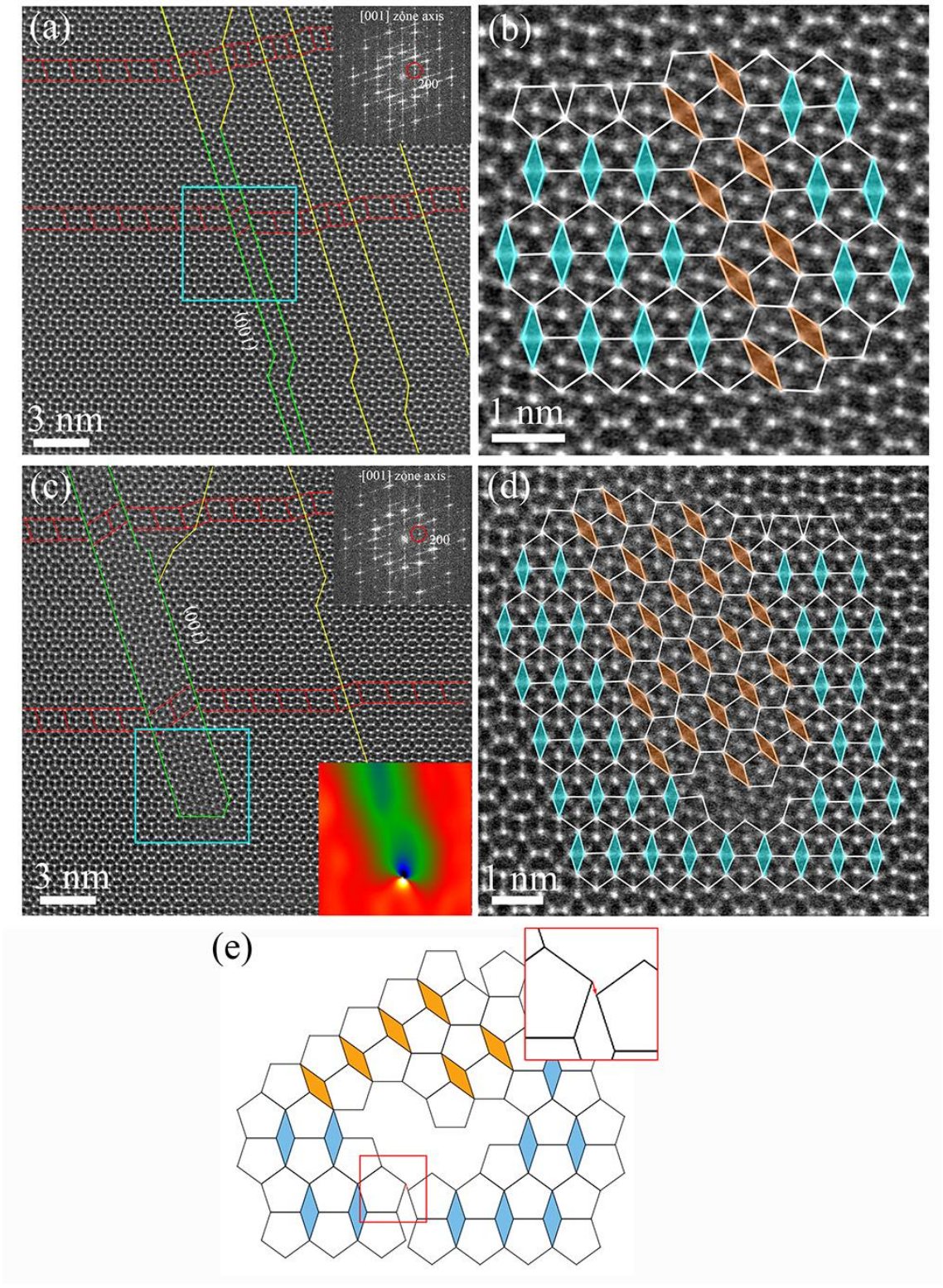

Fig. 4. (a and c) HAADF-STEM images of two planar defects with larger thickness (marked by green lines). (b and d) are enlarged HAADF-STEM images corresponding to the blue squares in (a) and (c), respectively. Stacking faults and twins are marked by green lines in (a) and (c) while APBs are indicated by yellow lines. The change of pentagon/rhomb tilting at stacking fault and twins are superimposed and highlighted in orange. Local g map of

the region marked by blue square in (c) is inserted in the bottom right of (c). It was obtained using the reflecting (200) plane marked by a red circle in the FFT of (c). (e) A Burgers circuit using unstrained tiles.

APBs have been observed in various super alloys or intermetallics, such as Ni (Co)-based single crystal super alloys [18], FeAl single crystals [19], Ni2MnGa-type Heusler alloys [20] and $TmAl_3$ intermetallics. It has been reported that the formation of APBs in a $ZrAl_3$ nano-precipitate are the consequence of successive shears with a/2<110> dislocations gliding on distinct (111) planes [21]. In the present work, recrystallization might occur during the 596°C heat treatment of the Al-/steel joint which could explain to the formation of ultrafine grains and extended defects such as APBs, stacking faults and nanotwins [22] . The origin of APBs can be attributed to the increase of the local stress during the 596°C heat treatment or friction melt bonding as the intermetallic compounds have a different thermal expansion compared to steel and aluminum [23]. Furthermore, In the presence of such small grain size, grain boundaries could act as preferential sites for the nucleation of APBs.

It has also been reported that the APBs could lead to stress homogenization through dislocation/APB interactions, resulting in a reduction of the tendency for intergranular failure in ordered IMs [24]. Due to the presence of APBs along with other microstructural defects, the desired high temperature mechanical properties could be achieved in FeAl and Fe_3Al [25]. Although Fe_4Al_{13} alone has limited direct applications, it has been widely utilized in metal matrix composite along with aluminum alloys [26]. Thus, developing more insight on the elastic and plasticity mechanisms in Fe_4Al_{13} is beneficial for many industrial applications. In the present work, the high density of APBs in the Fe_4Al_{13} IM is resulting from the presence of dislocations with large magnitude of Burgers vector (b/3[010], b=12.47 Å), leading to high stacking fault energy and making the formation of stacking faults and twins less energetically favorable. The combined effect of small grain size and the very high density of APBs could lead to outstanding strength/ductility balance. Further experimental efforts are needed to investigate the role of the ABPs observed in the

present work on the micromechanical response of the Fe_4Al_{13} IM. Special attention will have to be paid to the elementary dislocation/APB interaction mechanisms using in-situ TEM nanomechanical testing [27].

In summary, high density of APBs are formed in the Fe_4Al_{13} intermetallic of the Al-Fe welds after a heat treatment at 596°C. The formation of a high density of APBs transforms the Fe_4Al_{13} structure from the quasicrystal approximant to quasicrystal. Since Fe_4Al_{13} intermetallic is detrimental for the Al/steel weld performance due to its very low toughness, this new insight on the formation of large number of APBs merits to be further investigations as it has great potential to improve the toughness by increasing the strength/ductility balance.

Declaration of Competing Interest

The authors declare that they have no known competing financial interests or personal relationships that could have appeared to influence the work reported in this paper

Acknowledgements

T.S. acknowledges the financial support of National Fund for Scientific Research (FSR-FNRS), Belgium. A.S. and L.D. acknowledge the financial support of the European Research Council for a starting grant under grant agreement 716678, ALUFIX project. H.I. is mandated by the Belgian National Fund for Scientific Research (FSR-FNRS). This work was also supported by the Grant CDR–J011320F funded by FNRS and WALInnov ALFEWELD project (convention n°1710162) funded by the Service public de Wallonie Economie Emploi Recherche (SPW-EER).

References

[1] T. Tanaka, M. Nezu, S. Uchida, T. Hirata, Mechanism of intermetallic compound formation during the dissimilar friction stir welding of aluminum and steel, J.Mater. Sci. 55 (2019) 3064-3072.
[2] P. Matysik, S. Jóźwiak, T. Czujko, Characterization of low-symmetry structures from phase equilibrium of Fe-Al system—Microstructures and mechanical properties, Materials 8 (2015) 914-931.
[3] S. Korte-Kerzel, V. Schnabel, W.J. Clegg, M. Heggen, Room temperature plasticity in m-Al13Co4 studied by microcompression and high resolution scanning transmission electron microscopy, Scr.Mater. 146 (2018) 327-330.

[4] M. Dao, L. Lu, Y.F. Shen, S. Suresh, Strength, strain-rate sensitivity and ductility of copper with nanoscale twins, Acta Mater. 54 (2006) 5421-5432.
[5] Y.M. Eggeler, M.S. Titus, A. Suzuki, T.M. Pollock, Creep deformation-induced antiphase boundaries in L1 2 -containing single-crystal cobalt-base superalloys, Acta Mater. 77 (2014) 352-359.
[6] B. Wang, H. Idrissi, H. Shi, M.S. Colla, S. Michotte, J.P. Raskin, T. Pardoen, D. Schryvers, Texture-dependent twin formation in nanocrystalline thin Pd films, Scr.Mater. 66 (2012) 866-871.
[7] S. Chen, D. Yang, J. Yang, J. Huang, X. Zhao, Nanoscale structures of the interfacial reaction layers between molten aluminium and solid steel based on thermophysical simulations, J Alloy Compd. 739 (2018) 184-189.
[8] K.K. Fung, X.D. Zou, C.Y. Yang, Transmission electron microscopy study of Al13Fe4 tenfold twins in rapidly cooled Al–Fe alloys, Phil. Mag. Lett. 55 (1987) 27-32.
[9] K. Saito, K. Sugiyam, K. Hiraga, Al13M4-type structures and atomic models of their twins, Mater.Sci. Eng. A 294-296 (2000) 279-282.
[10] M. Heggen, L. Houben, M. Feuerbacher, Metadislocations in the structurally complex orthorhombic alloy Al13Co4, Phil. Mag. 88 (2008) 2333-2338.
[11] K.V. Vamsi, T.M. Pollock, A new proximate structure for the APB (111) in L12 compounds, Scr.Mater. 182 (2020) 38-42.
[12] M.J. Hÿth, L. Potez, Geometric phase analysis of high -resolution electron microscopy images of antiphase domains: Example Cu3Au, Phil. Mag. A 76 (1997) 1119-1138.
[13] C. van der Rest, P.J. Jacques, A. Simar, On the joining of steel and aluminium by means of a new friction melt bonding process, Scr.Mater. 77 (2014) 25-28.
[14] A. Simar, S. Godet, T.R. Watkins, Highlights of the special issue on metal additive manufacturing, Mater. Charact. 143 (2018) 1-4.
[15] T. Sapanathan, N. Jimenez-Mena, I. Sabirov, M.A. Monclús, J.M. Molina-Aldareguía, P. Xia, L. Zhao, A. Simar, A new physical simulation tool to predict the interface of dissimilar aluminum to steel welds performed by friction melt bonding, J Mater. Sci.Technol. 35 (2019) 2048-2057.
[16] N. Jimenez-Mena, P.J. Jacques, L. Ding, N. Gauquelin, D. Schryvers, H. Idrissi, F. Delannay, A. Simar, Enhancement of toughness of Al-to-steel Friction Melt Bonded welds via metallic interlayers, Mater.Sci. Eng. A 740-741 (2019) 274-284.
[17] P. Donnadieu, A. Proult, C. Ricolleau, The role of defects in the crystal/quasicrystal transformation, Bull. Mater. Sci. 20 (1997) 509-517.
[18] H. Long, Y. Liu, D. Kong, H. Wei, Y. Chen, S. Mao, Shearing mechanisms of stacking fault and anti-phase-boundary forming dislocation pairs in the γ′ phase in Ni-based single crystal superalloy, J Alloy Compd. 724 (2017) 287-295.
[19] H.Y. Yasuda, K. Nakano, T. Nakajima, M. Ueda, Y. Umakoshi, Effect of ordering process on giant pseudoelasticity in Fe3Al single crystals, Acta Mater. 51 (2003) 5101-5112.
[20] S.P.Venkateswaran, N.T.Nuhfer, M.D.Graef, Anti-phase boundaries and magnetic domain structures in Ni2MnGa-type Heusler alloys, Acta Mater. 55 (2007) 2621-2636.
[21] W. Lefebvre, N. Masquelier, J. Houard, R. Patte, H. Zapolsky, Tracking the path of dislocations across ordered Al3Zr nano-precipitates in three dimensions, Scr.Mater. 70 (2014) 43-46.
[22] J. Bystrzycki, J. Paszula, R.A. Varin, Structure and hardness of explosively loaded FeAl intermetallic alloys, Mater.Sci. Eng. A 239–240 (1997) 546–558.
[23] N. Jimenez-Mena, T. Sapanathan, J.M. Drezet, T. Pirling, P.J. Jacques, A. Simar, Residual stresses of friction melt bonded aluminum/steel joints determined by neutron diffraction, J Mater. Process. Tech. 266 (2019) 651-661.
[24] U.Prakash, R.A.Buckley, H.Jones, C.M.Sellars, On strain contrast from B2 antiphase domain boundaries in rapidly solidified Fe-32at%Al-15at% Mo alloy, Scri.Metall. 25 (1991) 2249-2253.

[25] U. Prakash, R. Buckley, H. Jones, C. Sellars, Structure and properties of ordered intermetallics based on the Fe-Al system, Isij Int. 31 (1991) 1113-1126.
[26] J.-M. Lee, S.-B. Kang, T. Sato, H. Tezuka, A. Kamio, Microstructures and Mechanical Properties of Al3Fe Reinforced Aluminum Matrix Composites Fabricated by a Plasma Synthesis Method, Mater. Trans. 43 (2002) 2487-2493.
[27] V. Samaee, M. Dupraz, T. Pardoen, H. Van Swygenhoven, D. Schryvers, H. Idrissi, Deciphering the interactions between single arm dislocation sources and coherent twin boundary in nickel bi-crystal, Nat. Commun.12 (2021) 962.